This is a preprint, the final version is subject to change, of the American Mineralogist (MSA)
Cite as Authors (Year) Title. American Mineralogist, in press.
(DOI will not work until issue is live.) DOI: http://dx.doi.org/10.2138/am-2016-5684

Revision 1

Location and Stability of Europium in Calcium Sulfate and its Relevance to Rare Earth Recovery from Phosphogypsum Waste

Radha Shivaramaiah,[1] Wingyee Lee,[1] Alexandra Navrotsky,[1] Dechao Yu,[2] Paul Kim,[2] Haohan Wu,[2] Zhichao Hu,[2] Richard Riman[2] and Andrzej Anderko[3]

[1] *Peter A. Rock Thermochemistry Laboratory and NEAT ORU, University of California Davis, Davis, California 95616*

[2] *Department of Materials Science and Engineering, Rutgers, The State University of New Jersey, 607 Taylor Road, Piscataway, New Jersey 08855*

[3] *OLI Systems, Inc., 240 Cedar Knolls Road, Suite 301, Cedar Knolls, New Jersey 07927*

ABSTRACT

Rare earth elements (REE) are technology drivers, essential for applications ranging from clean energy technologies to biomedical imaging. Thus they are "critical elements" and it is desirable to find additional RE domestic sources and explore green extraction technologies to overcome their supply risk. Phosphogypsum, a major byproduct of the phosphate fertilizer industry, incorporates a significant amount of RE from the apatite source rock and thus is a potential alternate source of RE. In order to know the accessibility and extractability of RE from phosphogypsum, it is important to understand the location and nature of RE binding. Here, we report the synthesis of analogs of RE doped phosphogypsum, with europium (Eu) as a model RE. Using several characterization tools we conclude that, the majority of Eu is on the surface of the calcium sulfate crystal as a separate secondary phase, namely a metastable amorphous/nanocrystalline precipitate in which Eu is associated with phosphate and sulfate as counterbalancing ions. The rapid precipitation at low temperature could be responsible for this behavior, which may not represent equilibrium, and our experiments are comparable in the time scale with the fast phosphogypsum precipitation in the industrial process. These results suggest that the Eu is not entrapped by ionic substitutions in the calcium sulfate lattice. Thus RE should be extracted relatively easily from phosphogypsum using methods that extract the RE from its surface.

Key Words: Phosphogypsum, rare earth elements, thermodynamics, spectroscopy.

INTRODUCTION

Rare earth elements (REE) are technologically very important in today's world. They are found in materials such as catalysts, batteries, magnets, phosphors, cell phones, LED displays, GPS equipment, night vision goggles, and many others (Cho et al. 1999; Gai et al. 2014; Bitnar et al. 2002; Shen et al. 2008; Zhou et al. 2008). REE, contrary to their name are moderately abundant in the earth crust; however there are few natural occurrences of ores in which REE are in concentrations of 1 wt% or greater (Lipin et al. 1989). The major commercial REE ores contain bastnaesite and monazite (Shivaramaiah et al. 2016; Ni et al. 1995; Glass et al. 1945). Currently the major and almost sole global producer and supplier of REE is China (Keith 2011; Scarce supply 2014), making RE supply vulnerable to geopolitical control (Humphries 2010). REEs are thus considered 'critical' or 'strategic' since their supply risk could adversely affect today's technology-dependent society across the globe (Humphries 2010). This has called for a situation where there is an urgent need for strategic plans to manage the supply risk of REEs, which is one of the major focus areas of Critical Materials Institute, an Energy Innovation Hub established by the U. S. Department of Energy. Its strategy includes search for alternative sources of RE, from which they can be recovered economically.

Phosphate rock, which is used as a source for synthesizing soluble phosphoric acid-based fertilizers, contains an appreciable amount of RE (0.06 %) (Habashi 1985; Altschule et al. 1967). Its major mineral is apatite ($Ca_{10}(PO_4)_6(OH,F,Cl)_2$) (Waggaman et al. 1915). Since RE substitute easily for Ca, they are present within the lattice of apatite itself or in the associated monazite phase ($REPO_4$). In the wet processing of the ore, phosphate rock is treated with sulfuric acid to obtain phosphoric acid and a byproduct phosphogypsum as shown in equation (1) (Slack 1968; U.S. Geological Survey 2012).

$$Ca_5F(PO_4)_3 + 5H_2SO_4 + 10H_2O \rightarrow 3H_3PO_4 + 5CaSO_4 + 2H_2O + HF \quad (1)$$

During this process, ~ 38 wt% of RE from original rock are incorporated into the byproduct phosphogypsum while the rest remains in sludge (~12 wt%, obtained by evaporative concentration of phosphoric acid) and in clay (~ 40 wt %) (Thyabat and Zhang 2015). Thus, both phosphogypsum and sludge could be potential attractive sources of RE. Phosphogypsum and sludge comprise hydrated forms of $CaSO_4$ with some occluded phosphate phases. Every year 220 million tons of phosphate rock are mined and processed worldwide to produce agricultural fertilizer (Hull and Burnett 1996). For every ton of phosphate rock processed, 5 tons of phosphogypsum are produced (Tayibi et al. 2009). Despite its use in agriculture, construction materials and road building (Yang et al. 2009; Smadi et al. 1999), a large excess remains, including much whose radium concentration exceeds the EPA standard (10 pCi/g), precluding industrial reuse (Hull and Burnett 1996; Rutherford et al. 1995). Such phosphogypsum is stacked into piles, which occupy hundreds of acres near these fertilizer plants, especially in Florida (Lottermoser 2010). These stacks are currently treated as waste and have been stored for decades now, causing serious ecological concern. In order to target 'stack free' conditions in the fertilizer plants, it is important to aim at a safe and sustainable use of phosphogypsum and to look at it as a potential resource rather than a waste (Hilton 2010). While phosphogypsum and sludge are indeed dilute sources of REs (as are many so-called rare earth ores), recovering REE from them will have additional benefits as it will aid in removing potentially hazardous waste and eventually transform phosphoric acid production to a low waste process. A case study of evaluation of REE recovery (Kulczycka et al. 2016) from phosphogypsum in one of the plants in Poland shows that RE recovery from phosphogypsum is cost-effective in operation but requires

significant initial financial investment. It is however characterized by a relatively high degree of risk due to the volatility of prices of RE.

In order to optimize extraction of RE from phosphogypsum, it is essential to know where they are incorporated in these solids and to understand the nature of their binding and thermodynamic stability. Some of the possibilities are: (a) RE could form solid solution in gypsum by substituting for Ca – without charge balancing by vacancy creation or with charge balancing by phosphate, or other ions, (b) RE could be surface adsorbed and (c) RE could form auxiliary phases, either amorphous or crystalline, on gypsum surfaces or in between gypsum grains. In each of these circumstances, the degree of accessibility and extractability of RE will vary significantly. Thus the main goal of this work is to determine the fate of RE when precipitated rapidly from a solution rich in Ca, SO_4 and PO_4.

The present study chose a simple synthetic model system, namely $CaSO_4$ with added phosphate and/or europium (Eu) to study RE location and stability. This system is more controllable than commercial phosphogypsum, which is variable in composition, phases present, and impurities. We chose Eu as a model RE because of its easy spectroscopic detection and characterization of local environment (Jagannathan and Kottaisamy 1995). By precipitation from aqueous solution, we synthesized gypsum samples with different Eu and phosphate concentrations. Using an array of characterization techniques (chemical analysis, thermal analysis, X-ray diffraction, scanning electron microscopy, infrared and photoluminescence spectroscopy, oxide melt solution calorimetry) we arrived at the likely location of Eu in the solid phase assemblage and determined the stability of these phases.

MATERIALS AND METHODS

Synthesis of Eu and phosphate doped $CaSO_4$. All the samples were synthesized by a simple co-precipitation reaction using europium nitrate (99.99 %, Alfa Aesar), calcium nitrate tetrahydrate (99.98 %, Alfa Aesar) and sodium sulfate (99.99 %, Alfa Aesar). Europium nitrate and calcium nitrate were dissolved in water to which sodium sulfate solution was added under mechanical stirring. The final solution was then aged at 80 °C (temperature typical of the reactor in the industrial fertilizer process) for 24 h. The precipitate was separated by centrifugation and the sample was washed with deionized (DI) water three times to remove sodium and nitrate ions. The product was then dried in an oven at 80 °C. For the synthesis of samples with phosphate, ammonium diphosphate (99.99 %, Sigma Aldrich) solution was added as a source of phosphate during the initial precipitation. Since we used $Eu(NO_3)_3$ as a source of Eu in the synthesis in which Eu in +3 oxidation state and since in the course of synthesis there were no reducing conditions, we do not expect Eu to change its oxidation state. Indeed the spectroscopic studies (see below) confirmed Eu^{3+}. The concentration of the dopants in solution (Eu^{3+}, PO_4^{3-}) was between 0.01 - 0.5 moles per mole of calcium sulfate. The lowest concentration of 0.01 mol Eu^{3+}/PO_4^{3-} was chosen since it is close to the RE concentration in natural phosphate rock and in phosphogypsum. Several concentrations above 1 mol % were chosen, as the concentration of RE and phosphate is higher in sludge. The wide range in dopant concentration also allows us to seek systematic trends in the structure and stability. For all the nominal concentration of Eu in solution, two sets of Eu doped $CaSO_4$ were synthesized – one without any phosphate where the excess sulfate serves as a counter ion and the other with phosphate where phosphate, in addition to sulfate could act as a charge balancing anion. Furthermore the behavior of Eu in the solid in the presence and absence of phosphate also aided in understanding RE behavior both in the

125 phosphogypsum stacks and sludge. In this paper, we have focused on four samples; each made
126 from solutions with 0.01 and 0.5 mol dopants per mol of calcium sulfate (see Table 1).
127 **Characterization**. Powder X-ray diffraction patterns (XRD) of the synthesized samples were
128 recorded using a Bruker AXS D8 Advance diffractometer with CuKα radiation, (Kα = 1.5418 Å)
129 to identify the phases. Data were collected in the 2θ range of 10 –70□° with a step size of 0.02°
130 2θ and a collection time of 0.5 s/step using a zero-background sample mount. The Rietveld
131 technique was employed for structure refinement of all the samples using X'pert HighScore Plus
132 software. All the structure refinements were carried out using the published structure models of
133 gypsum and bassanite. For samples containing a mixture of bassanite and gypsum, two-phase
134 refinements were performed to obtain the phase ratio. Thermogravimetric analysis (TGA) was
135 performed to determine the water content in the samples using a Setaram Labsys thermal
136 analysis system in a dynamic Ar atmosphere (25 - 500 °C, 5 °C/min, Pt crucible, and 10 cc/min).
137 The data were analyzed using Calisto software (Version 1.31). The overall RE content in the
138 samples was measured by ICP-MS with an Agilent Technologies' 7500a instrument. A known
139 amount of sample was dissolved in ~0.1 mL of ICP grade HCl and diluted with Millipore water
140 (Simplicity® Systems). Attenuated total reflectance-Fourier transform infrared (ATR - FTIR)
141 spectra of all the samples were recorded using a Bruker Model Alpha-P IR spectrometer
142 (diamond ATR cell, 4 cm^{-1} resolution, 400 - 4000 cm^{-1}). Morphology, phase segregation and
143 composition heterogeneity of all the samples, was examined by scanning electron microscopy
144 (SEM) and energy dispersive spectroscopy (EDS) using a JEOL 7401 SEM at Lawrence
145 Livermore National Laboratory, operated at 3 kV for imaging and 15 kV for chemical analysis.
146 Photoluminescence spectroscopy (PLS) was performed with a high-resolution
147 spectrophotometer, (Edinburgh FLS920) using a xenon lamp as the excitation source, to examine

148 emission from Eu in different sites in the sample. High temperature oxide melt solution
149 calorimetry was performed using a custom built isoperibol Tian-Calvet microcalorimeter. The
150 details of the calorimetry used are described elsewhere (Navrotsky 1977; Navrotsky 1997).
151 Molten sodium molybdate was used as a solvent at 700 °C. Heats of drop solution of the binary
152 oxides were taken from previously published work (Navrotsky 2014; Majzlan et al. 2002; Drouet
153 and Navrotsky 2003; Ushakov 2001).

154 **RESULTS**

155 Compositions of all four samples obtained using ICP analysis is listed in Table 1. Based
156 on the ICP analysis and water content obtained by TG we arrive at a molecular formula for each
157 sample. The results confirm that both Eu and phosphate are incorporated into the solid during the
158 precipitation reaction. However the amount incorporated in the solid is only about 50 % of that
159 in the initial solution or even less. In all the samples the ratio of S to Ca exceeds 1, indicating
160 that the excess sulfate could form phases with cations other than Ca, perhaps Eu and Na.
161 In samples doped with both europium and phosphate, the ratio of Eu to P exceeds 1 as well,
162 indicating that, besides forming a phase with phosphate, Eu also forms other phases, perhaps
163 with sulfate from the observations noted above.

164 PXRD patterns of all the four samples are shown in Figure 1. All the samples contained
165 either one or both of the hydrated phases of $CaSO_4$ (gypsum – $CaSO_4 \cdot 2H_2O$ and bassanite –
166 $CaSO_4 \cdot 0.5H_2O$). Two – phase Rietveld refinements were performed in order to quantify the two
167 hydrated phases of $CaSO_4$ in each sample (Supporting information, SI 1). Gypsum crystallizes in
168 orthorhombic structure and bassanite in trigonal. Samples with a lower amount of Eu and PO_4 –
169 GS 1 and PG1 comprised gypsum as the major phase, consistent with the literature reports on Eu
170 doped $CaSO_4$ (Jagannathan 1995). The PXRD pattern corresponding to GS 1 could be fit with

171 the gypsum phase alone, and that of PG 1 with a mixture of gypsum (88 %) and bassanite (12
172 %). GS 2 and PG 2, on the other hand, were a mixture of gypsum and bassanite. Phase fractions
173 obtained by the Rietveld analysis are listed in Table 2. No shifts in the Bragg reflections were
174 observed in the gypsum or bassanite phase, in any of the samples that might have been due to
175 incorporation of Eu and PO_4 during the precipitation. Further, no additional peaks corresponding
176 to auxiliary phases containing Eu, phosphate, or other elements were detected. This indicates that
177 any auxiliary phases present were either in too small amounts to be detected or too poorly
178 crystalline or amorphous to observe in the PXRD.

179 TG-DSC curves obtained for all the samples are shown in Figure 2. All the samples
180 exhibit mass loss between 100 – 250 °C, which is endothermic and can be attributed to
181 dehydration of calcium sulfate phases. An exothermic peak is observed in all the samples at ~370
182 – 400 °C, which is not associated with any mass loss. A subsequent TG-DSC run on the same
183 sample in all the cases showed disappearance of the exothermic peak. This indicates that the
184 exothermic process observed at ~370 °C is irreversible and we believe, it could be associated
185 with the crystallization of any amorphous secondary phases present in these samples. XRD
186 patterns of the heat treated samples are given in supporting information SI 2 and showed peaks
187 corresponding to anhydrite, confirming calcium sulfate dehydration. However, no peaks for
188 crystalline phases containing Eu or phosphate were observed, perhaps because they were present
189 in too low concentration. In each case, depending on the phase fraction obtained by Rietveld
190 analysis, total water content calculated from mass loss between 100 – 250 °C, was distributed
191 among gypsum and bassanite (Table 2). The remaining excess water is probably loosely bound
192 water on the surfaces and between the particles or probably is the water associated with any
193 possible amorphous phases. It can be seen that the presence of Eu and phosphate affects the

194 water content incorporated in the solid and in turn the phase fractions of gypsum and bassanite in
195 all the cases. Both with and without phosphate, when the Eu content is lower, most of the water
196 is associated with $CaSO_4$ and a tiny fraction of it is in excess, whereas with higher Eu content, a
197 larger fraction of water is in excess. This is indirect evidence for the possible presence of
198 hydrated amorphous phases containing Eu.

199 ATR spectra of the four samples under study are shown in Figure 3. The spectrum of GS
200 1 sample exhibits similar features as that of pure gypsum, where the symmetry of sulfate is
201 reduced from T_d to C_{2v}. Peaks due to sulfate were observed at 1117 cm^{-1} – ν_3, 1003 cm^{-1} – ν_1 and
202 667 cm^{-1}, 600 cm^{-1} – ν_4. However, GS 2, with higher Eu concentration exhibits additional
203 features. We observe a broad band at 1103 cm^{-1} (ν_3) with a shoulder at 1000 cm^{-1} (ν_1). ν_4 appears
204 as a doublet at 650 cm^{-1} and 590 cm^{-1}. Unlike in GS 1 and pure gypsum, the broad band observed
205 in the case of GS 2 arises due to overlapping of several peaks which could be due to sulfate
206 associated in two different coordination symmetries, possibly with Ca and Eu. Though this
207 sample comprises both gypsum and bassanite, sulfate in both these phases is known to be in
208 similar environments and the stretching and bending modes of sulfate is known to be identical in
209 them (Bishop 2014). A tiny peak at 503 cm^{-1} corresponds to ν_2, symmetric bending mode and a
210 tiny band at 430 cm^{-1} corresponds to Eu-O lattice vibrations. Observation of Eu-O vibrations and
211 broad band with several overlapping peaks thus suggests that sulfate in GS 2 is associated with
212 more than one coordination symmetry. On the other hand, both sulfate and phosphate being
213 tetrahedral, their stretching and bending modes overlap with each other and it is hard to
214 differentiate among them in the samples with phosphate. The ATR spectrum of PG 1 exhibits a
215 band at 1149 cm^{-1} with a shoulder at 1117 cm^{-1} which can be attributed to ν_3 mode of sulfate
216 and/or phosphate. A doublet observed at 667 cm^{-1} and 600 cm^{-1} corresponds to the ν_4 bending

mode and features observed below 500 cm^{-1} could be due to Eu-O vibrations. Unlike in PG 1, in PG 2 the concentration of Eu is high, and it is associated with both sulfate and phosphate. Thus, the spectrum for PG 2 is a sum of vibrations due to phosphate and sulfate associated with Ca and Eu. A broad band observed at 1103 cm^{-1} (ν_3) with a shoulder at 1001 cm-1 (ν_1) could arise due to several overlapping peaks arising due to S-O and P-O asymmetric stretching vibrations of phosphate and sulfate associated with Ca and Eu. Features observed at 619 cm^{-1}, and 595 cm^{-1} could be a attributed to ν_4 bending mode of sulfate, whereas the one observed at 537 cm^{-1} could be attributed to ν_4 bending mode of phosphate. All the four samples exhibit a doublet at ~3500-3380 cm^{-1} corresponding to stretching vibration modes of water and a doublet at ~1680 and 1620 cm^{-1} corresponding to bending mode of water. The stretching modes at 3500-3380 cm^{-1} are sharp in GS 1 and PG 1 where the bassanite phase is minor and the adsorbed water content is low. In the case of GS 2 and PG 2, the peaks are broad and additionally there is a shift in the peaks with reversal in the intensities of ν_1 and ν_3 modes of water. This could be due to the presence of both gypsum and bassanite in these samples and also the higher amount of adsorbed water. Gypsum is known to have peaks at 3395 (ν_1-H_2O) and 3489 cm-1 (ν_3-H_2O), whereas bassanite at 3553 (ν_1-H_2O) and 3605 cm^{-1} (ν_3-H_2O) corresponding to stretching modes of water (Liu 2009).

SEM images of the four samples are shown in Figure 4. Two different crystal morphologies were found across all the samples - one which was lath-like or acicular with size between 20 to 120 μm and the other consisting of platelets with size between 40 and 80 μm. These two morphologies for calcium sulfate have been previously described in the literature (Kovler1998; Shih et al. 2005). In addition, in the case of samples with phosphate; we observe a layer of particles without any faceted morphology forming a thin coating on the surface of the crystals (Figure 5a). EDS revealed that the layer was composed of 50.3 % wt O, 16.9 % wt Ca,

240 13.5 % wt S, 16.5 % wt Eu and 2.8 % wt P. The molar ratio between Eu and P in these particles
241 on surface is thus ~1.2, with a likely uncertainty of about 10 - 20 %. This suggests that europium
242 in this thin surface layer is associated with phosphate, forming a separate Eu rich phase, that
243 possibly could be europium phosphate, $EuPO_4$, or a hydrated variant. This is also supported by
244 the TG and IR observations, where we observe excess adsorbed water. In addition, small
245 particles of around 1 μm diameter were found on the surface of the flat platelet crystals in both
246 PG1 and PG2 which is shown in Figure 5. Under a higher magnification 30,000 - 40,000 x, it
247 was clear that the morphology of these smaller particles were different from the larger platelets
248 and thin crystals. They had no faceted shape and resembled clusters of tiny spherical units that
249 were agglomerated together. The visual estimation of the concentration of these clusters was 1 –
250 2 %. EDS revealed that these clusters were Eu rich, ranging from 10 to 50 wt. % while the P
251 ranged from 0.5 to 2.5 wt. %. The mole ratio of Eu to P varied from 1.4 to 1.7 in these particles,
252 indicating that europium was not only associated with phosphate but also could be forming other
253 auxiliary phases, perhaps europium sulfate or oxide or hydroxide. Thus SEM images confirm
254 that, in these solids Eu forms auxiliary phases. While the Eu-rich phases were not detected by
255 XRD, they were distinguishable from gypsum/bassanite phases based on their morphology and
256 composition in SEM. The observations that these auxiliary phases appear to be thin surface
257 coatings on the crystals and that particles were aggregates of tiny spherical units, indicate that
258 even if they were to produce Bragg reflections they would be broad and will be buried under the
259 strong peaks from gypsum/bassanite.

260 Photoluminescence spectra (PLS) of all the four samples are shown in supporting
261 information SI 3. The samples with lower Eu concentrations, GS 1 and PG 1, did not exhibit any
262 significant peaks in the PLS. However the samples with higher Eu concentration, GS 2 and PG 2

exhibit distinct emission spectra which are consistent with trivalent Eu. GS 2 has the maximum emission band centered at 612 nm, which is due to the $^5D_0 \rightarrow {}^7F_2$ electric dipole transition of Eu^{3+}, while PG 2 exhibits the maximum emission peak at 593 nm, which is due to $^5D_0 \rightarrow {}^7F_1$ magnetic dipole allowed transition of Eu^{3+}(Du 2011; Sun 2010). For GS 2, the $^5D_0 \rightarrow {}^7F_2$ emission intensity is much stronger than the $^5D_0 \rightarrow {}^7F_1$ emission intensity, which indicates that the Eu^{3+} is located at a site without inversion symmetry, like in $Eu_2(SO_4)_3.xH_2O$ host (see SI4 for the PLS of commercial $Eu_2(SO_4)_3.xH_2O$). However for PG 2 the reverse case is observed, due to decrease in the contribution of $^5D_0 \rightarrow {}^7F_2$ emission with the introduction of PO_4^{3-} groups, likely forming the auxiliary phase $EuPO_4$ (see SI4 for the PLS of commercial $EuPO_4$ for comparison). These results reveal that at higher Eu concentrations, in the absence of phosphate Eu is largely associated with SO_4^{2-} group, but in the presence of phosphate Eu is largely associated with PO_4^{3-} group. Thus Eu probably exists as $Eu_2(SO_4)_3$ and $EuPO_4$ in the case of GS 2 and PG 2, respectively, although these phases may be poorly crystalline (nanophase or amorphous) and/or hydrated. PLS of industrial phosphogypsum does not exhibit any features corresponding to RE emission, which is similar to our observation in the case of GS 1 and PG 1.

High temperature oxide melt solution calorimetric measurements were made on these samples to examine their energetic stability. Enthalpy of formation values were calculated from different constituents in order to determine the relative stability of these phases; (a) from a mixture of oxides and water, (b) from mixture of anhydrous sulfates, phosphate and water and (c) from mixture of hydrated sulfates, phosphate. The thermochemical cycle used to calculate enthalpy of formation from a mixture of anhydrous sulfates, phosphate and water is shown in Figure 6; other cycles are analogous. Enthalpies of drop solution of all the constituents used in a

285 thermochemical cycle for calculation of formation enthalpies are listed in Table 3. The calculated
286 enthalpy of formation values from different constituents is listed in Table 4.

287 The enthalpy of formation values calculated from oxides for all four samples are highly
288 exothermic, indicating that these phases are stable compared to the oxides of their constituent
289 metals. This however reflects the highly exothermic formation of sulfates and phosphates and
290 does not provide useful insights into relative stability of these phases. We therefore calculated
291 the enthalpy of formation of Eu-doped gypsum-phosphogypsum phases from a mixture of
292 anhydrous sulfates, Eu-phosphate and water. While all the constituent sulfates exist in hydrated
293 form, we opt to calculate formation enthalpy values from anhydrous sulfates, as there was not
294 enough total water content in each sample to attribute to hydrated forms of constituent sulfates
295 ($CaSO_4$, $Eu_2(SO_4)_3$ and Na_2SO_4). These values are negative for GS 1 and PG 1 but slightly
296 positive for GS 2 and PG 2, indicating that samples with low Eu concentration are
297 thermodynamically more stable than samples with higher concentration of Eu. However, it is
298 important to realize that in all these samples water is associated with $CaSO_4$, which exists as
299 gypsum and bassanite. The small negative enthalpy observed for the two low concentration
300 samples could therefore arise due to attributing all the water molecules to loosely held water.
301 Since we do not observe any auxiliary phases in XRD corresponding to Eu or Na, we had no
302 choice but to distribute the water molecules between thermodynamically more stable phases of
303 $CaSO_4$ – gypsum and bassanite. The remaining water was attributed to loosely bound water,
304 which could be associated with amorphous phases or held between the particles. Phase fractions
305 of gypsum and bassanite were obtained by combined Rietveld analysis of PXRD pattern and TG
306 results as described earlier in the text and listed in Table 2. We calculated the formation
307 enthalpies of all the four synthesized samples from a mixture of gypsum, bassanite and other

sulfates / phosphates and the values obtained are listed in the last column of Table 4. The values are all positive, indicating that all the synthesized samples are energetically metastable with respect to the stable hydrated polymorphs of $CaSO_4$ and other crystalline phases containing Eu, sulfate and phosphate. The metastability increases with increasing Eu content. We suspect this reflects the presence of amorphous phases as argued from TEM and XRD evidence. The calorimetric data thus support the other evidence including SEM, ATR, PLS and TG-DSC that Eu and P are not present as stable solid solutions or as stable secondary phases but more likely are present as metastable nanophase or amorphous precipitates on the surfaces of gypsum or bassanite.

DISCUSSION

Various experimental techniques adopted to examine the nature of Eu in the synthetic gypsum/phosphogypsum thus indicate that it likely forms metastable amorphous precipitates on the major solid sulfate phases. The precipitate formed was found to have Eu associated with both phosphate and sulfate. It is important to note that, quite similar to our observations with the synthetic samples, industrial phosphogypsum also does not exhibit any rare earth rich auxiliary phases in XRD and it exhibits an exothermic peak at 350 °C in DSC which is often attributed to crystallization of amorphous impurity phases (Hanna 1999). Further, similar amorphous coatings were observed under SEM on the surface of larger platelets of the industrial samples. Thus the results obtained here for the location of Eu are likely to be the same for REs in the industrial phosphogypsum. Therefore the RE are likely to be in the form of surface adsorbed metastable auxiliary phases in the phosphogypsum stacks. Industrial phosphogypsum stacks from Florida are rich in Nd, Ce, La and Y. While the results obtained in the current work are based on only Eu, it could probably be generalized to other RE since they all possess similar properties, which

is the reason for finding them together in nature. However, there could be some variations in behavior among different RE, which prompt us for future work with Nd and Y, which are abundant in industrial samples. It would also be interesting to examine the behavior of RE in the solid precipitated from a solution with a mixture of RE. Thermodynamic stability of individual RE sulfates and phosphates might dictate phase formation in such a situation.

The other important observation in this work is the difference in RE behavior in the samples precipitated from solutions with and without phosphate. We see that, in the samples precipitated without phosphate in solution, Eu is mainly associated with sulfate, while in samples with phosphate in solution during the precipitation, Eu is associated with both sulfate and phosphate ions. However, in both cases most of the Eu forms auxiliary amorphous/nanophase precipitates though one cannot exclude the possibility of a very small amount of RE being in the $CaSO_4$ lattice. We suspect that the rapid precipitation at low temperature is responsible for this behavior. The goal of this study was to mimic the industrial precipitation conditions and we are careful not to claim equilibrium. It is possible that, at equilibrium, a greater extent of RE ionic substitution within the gypsum crystal structure might occur. A separate study, probably involving hydrothermal or high temperature annealing conditions, would be necessary to probe kinetic versus thermodynamic control and to establish and prove equilibrium and that is outside the scope of the present work.

The observed surface precipitation has an important implication for RE recovery from byproducts of phosphate ore processing. The formation of metastable phases and their location on surfaces make them more accessible to dissolution.

Both phosphogypsum and sludge obtained at various stages of soluble phosphate synthesis are significant sources of RE. Phosphogypsum, which incorporates ~38 % of REs from the original phosphate rock, has a very low concentration of phosphate and hence the majority of RE could be associated with sulfate. However the sludge obtained after evaporating phosphoric acid to P_2O_5 is obviously rich in phosphate and thus RE in sludge could be associated with both sulfate and phosphate phases. Although the sludge incorporates only ~12 % of REs from the original rock, the overall concentration of RE in sludge is much higher than in phosphogypsum. While the sludge has bassanite ($CaSO_4 \cdot 0.5H_2O$) as a major phase, gypsum ($CaSO_4 \cdot 2H_2O$) is the major phase in phosphogypsum. A similar difference is also observed in the synthetic samples in the present work, where gypsum is the major phase in samples with lower Eu concentration and bassanite is the major phase in samples with higher Eu concentration. It is not clear whether the higher RE concentration acts, kinetically or thermodynamically, to select for a given calcium sulfate phase. In both laboratory and industrial samples it would appear that enough water is present during synthesis to form the dihydrate, so the reason for bassanite formation is not obvious.

IMPLICATIONS

Eu-doped gypsum and phosphogypsum analogs were prepared in the laboratory to examine the location and stability of Eu in these phases. While no Eu-rich phases were observed by XRD, the other techniques including SEM, TG-DSC and high temperature oxide melt solution calorimetry collectively indicate that the Eu in gypsum/phosphogypsum exists as a poorly crystalline nanophase or amorphous secondary phase which is energetically metastable. The phosphogypsum precipitation in the industrial process occurs fast so our experiments are comparable in time scale. The similarities that we observe in PXRD and SEM of industrial

samples and the synthetic samples support the relevance of our experiments to the industrial process. The accessibility of RE to leaching/extraction should thus be high as they exist as small particles of an energetically metastable secondary phase on grain surfaces rather than being a part of the gypsum structure.. These observations are encouraging in terms of developing a commercially viable process for recovering RE from phosphogypsum and sludge.

ASSOCIATED CONTENT

A plot of TG-DSC, PXRD of heat treated samples, ATR spectra and PLS spectra of all the four samples is available in the supporting information

ACKNOWLEDGEMENTS

This work is supported by the Critical Materials Institute, an Energy Innovation Hub funded by the U.S. Department of Energy, Office of Energy Efficiency and Renewable Energy, Advanced Manufacturing Office. Authors thank Dr. Annie Kresting and Dr. Zurong Dai at Lawrence Livermore National Laboratory for SEM-EDS measurements.

References

Altschuler, Z. S., Berman, S., Cuttitta, F. (1967) Rare earths in phosphorites- geochemistry and potential recovery, Intermountain Association of Geologists - Fifteenth Annual Field Conference, 125-135

Bishop, J. L., Dyar, M.D., Swayze, G. A. (2014) Spectral properties of Ca-sulfates: gypsum, bassanite and anhydrite. American Mineralogist, 99, 2105-2115.

Bitnar, B., Durisch, W., Mayor, J.C., Tschudi, H. R. (2002) Characterization of rare earth selective emitters for thermophotovoltaic applications, Solar Energy Materials and Solar Cells, 73, 221–234

Cho, S. Y., Kim, I. T., Hong, K. S. (1999) Microwave dielectric properties and applications of rare-earth aluminates, Journal of Materials Research, 14, 114-119

Critical Materials Institute website; http://www.webcitation.org/6eOJErRbt, accessed on Jan 8, 2016

Drouet, C., Navrotsky, A. (2003) Synthesis, characterization and thermochemistry of K-Na H_3O jarosites. Geochimica et Cosmochimica Acta, 67, 2063-2076

Du, F. P., Nakai, Y., Tsuboi, T. J., Huang, Y. L., Seo, H. J. (2011) Luminescence properties and site occupations for Eu^{3+} ions doped in double phosphates $Ca_9R(PO_4)_7$ (R = Al, Lu). Journal of Materials Chemistry, 21, 4669-4678.

Gai, S., Li, C., Yang, P., Lin, J. (2014) Recent progress in rare earth micro/nanocrystals: Soft chemical synthesis, luminescent properties, and biomedical applications, Chemical reviews, 114, 2343–2389

Glass, J. J., Smalley, R. G. (1945) Bastnaesite. American Mineralogist, 30, 601-615

Habashi, F. (1985) The recovery of the lanthanides from phosphate rock, Journal of Chemical Technology and Biotechnology, 35A, 5-14

Hanna, A. A., Akarish, A. I. M., Ahmed, S. M. (1999) Phosphogypsum: Part I: Mineralogical, thermogravimetric, chemical and infrared characterization. Journal of Materials Science and Technology, 15, 431-434.

Hilton, J. (2010) Phosphogypsum: Use and Current Handling Practices Worldwide. http://www.webcitation.org/6eOHGnQrS, Accessed on Jan 8, 2016.

Hull, C. D., Burnett, W. C. (1996) Radiochemistry of Florida phosphogypsum. Journal of Environmental Radioactivity, 32, 213-238.

Humphries, M. (2010) Rare Earth Elements: The Global Supply Chain: Congressional Research Service; The Library of Congress: Washington, DC, USA

International phosphogypsum working group. http://www.webcitation.org/6eOGjLo7j Accessed on Jan 8, 2016.

Jagannathan, R., Kottaisamy, M. (1995) Eu^{3+} luminescence: a spectral probe in $M_5(PO_4)_3X$ apatites (M = Ca or Sr; X = F^-, Cl^-, Br^- or OH^-). Journal of Physics: Condensed Matter, 7, 8453–8466

Keith, R. L. (2011) Principal rare earth elements deposits of the U. S.: A Summary of domestic deposits and a global perspective. U.S. Geological Survey Scientific Investigations Report 2010–5220, 96, p: **1-96**. Available at http://www.webcitation.org/6eOGoCpl3 Accessed on Jan 8, 2016.

Kovler, K. (1998) Setting and hardening of gypsum-portland cement-silica fume blends, Part 2: Early strength, DTA, XRD, and SEM observations, Cement and concrete research, 28, 523-531.

Kulczycka, J., Kowalski, Z., Smol, M., Wirth, H. (2016) Evaluation of the recovery of rare earth elements (REE) from phosphogypsum waste e case study of the WIZOW chemical plant (Poland). Journal of Cleaner Production 113, 345-354

Lipin, B.R., Mckay, G.A. (1989) Geochemistry and mineralogy of rare earth elements. Mineralogical Society of America, 21, 259-302

Liu, Y., Wang, A., Freeman, J. J. (2009) Raman, MIR and NIR spectroscopic study of calcium sulfates: gypsum, bassanite and anhydrite. 40th Lunar and Planetary science conference, 2128

Lottermoser, B.G., (2010) Mine Wastes: Characterization, Treatment and Environmental Impacts. Springer-Verlag, Germany.

Majzlan, J., Navrotsky, A., Neil, J. M. (2002) Energetics of anhydrite, barite, celestine, and anglesite: A high-temperature and differential scanning calorimetry study. Geochimica et Cosmochimica Acta, 66, 1839-1850

Navrotsky, A. (1997) Progress and new directions in high temperature calorimetry revisited. Physics and Chemistry of Minerals, 24, 222-241

Navrotsky, A. (2014) Progress and new directions in calorimetry: A 2014 Perspective. Journal of American Ceramic Society, 97, 3349-3359

Navrotsky, A. (1977) Progress and new directions in high temperature calorimetry, Physics and Chemistry of Minerals, 2, 89-104

Ni, Y., Hughes, J. M., Mariano, A. N. (1995) Crystal chemistry of the monazite and xenotime structures. American Mineralogist, 80, 21-26

Phosphogypsum and the EPA ban. http://www.fipr.state.fl.us/about-us/phosphate primer/phosphogypsum-and-the-epa-ban/. Accessed on Jan 8, 2016.

Rutherford, P. M., Dudas, M. J., Arocena, J. M. (1995) Radioactivity and elemental composition of phosphogypsum produced from three phosphate rock sources, Waste Management & Research, 13, 407-423

Scarce supply - the world's biggest rare earth metal producers. 2014; http://www.webcitation.org/6eOI9rANJ. Accessed on Jan 8, 2016.

Shen, J., Sun, L-D., Yan, C-H. (2008) Luminescent rare earth nanomaterials for bioprobe applications. Dalton Transactions, 42, 5687–97

Shih, W.Y., Rahardianto, A., Lee, R. W., Cohen, Y. (2005) Morphometric characterization of calcium sulfate dihydrate (gypsum) scale on reverse osmosis membranes. Journal of Membrane Science, 252, 253-263

Shivarmaiah, R., Anderko, A., Riman, R., Navrotsky., A. (2016) Thermodynamics of bastnaesite – A major rare earth ore mineral. American Mineralogist, in press (DOI:http://dx.doi.org/10.2138/am-2016-5565)

Slack, A.V., (1968) Phosphoric Acid, Parts I and II, Marcel Dekker, New York.

Smadi, M.M., Haddad, R.H., Akour, A.M. (1999) Potential use of phosphogypsum in concrete. Cement and Concrete Research, 29, 1419–1425.

Sun, D. H., Zhang, J. L., Sun, D. X. (2010) Synthesis and spectral characterization of $EuPO_4$ and $LaPO_4$: Eu nanorods. Journal of Nanoscience and Nanotechnology, 10, 1782-1787.

Tayibi, H., Choura, M., López, F. A., Alguacil, F. J., Delgado, A. L. (2009) Environmental impact and management of phosphogypsum. Journal of Environmental Management, 90, 2377–2386.

Thyabat, S., Zhang, P (2015) REE extraction from phosphoric acid, phosphoric acid sludge, and phosphogypsum. Mineral Processing and Extractive Metallurgy, 124:3, 143-150

U.S. Geological Survey. (2012) Phosphate rock statistics and Information. Mineral Commodity Summaries, 118-119.

Ushakov, S. V., Helean, K. B., Navrotsky, A. (2001) Thermochemistry of rare-earth orthophosphates. Journal of Materials Research, 16, 2623-2633

Waggaman, W. H. Fry, W.H (1915) Phosphate rock and methods proposed for its utilization as a fertilizer. United States Department of Agriculture, Bulletin No 132.

Yang, J., Liu, W., Zhang, L., Xiao, B. (2009) Preparation of load-bearing building materials from autoclaved phosphogypsum. Construction and Building Materials, 23, 687–69

Zhou, Z., Hu, H., Yang, H., Yi, T., Huang, K., Yu, M. (2008) Up-conversion luminescent switch based on photochromic diarylethene and rare-earth nanophosphors. Chemical Communications, 39, 4786–4788

491

492 **Figure Captions**

493 **Figure 1.** PXRD patterns of all the samples stacked with the simulated patterns of gypsum and
494 bassanite

495 **Figure 2.**TG-DSC curves of Eu doped gypsum and phosphogypsum samples

496 **Figure 3.** ATR spectra of all the four samples

497 **Figure 4.** SEM images of (a) GS 1, (b) GS 2, (c) PG 1 and (d) PG 2

498 **Figure 5.** SEM image of PG 2 sample showing surface adsorbed layer of Eu phase and that of
499 PG 1 sample showing Eu – rich particles with no faceted morphology

500 **Figure 6.** Thermochemical cycle used for the calculation of enthalpy of formation values of Eu-
501 gypsum samples from a mixture of anhydrous sulfate and water

502

503

504

505

506

507

508

509 **Table 1**. Compositional analysis of all the four samples obtained by ICP analysis and TG
510 measurements.

Sample	Eu content in solution (mol per mol of $CaSO_4$)	PO_4 content in solution (mol per mol of $CaSO_4$)	Empirical formula (based on ICP and TG results)
GS1	0.01	0	$CaEu_{0.0012}Na_{0.28}(SO_4)_{1.14}\cdot 2.05H_2O$
GS2	0.5	0	$CaEu_{0.29}Na_{0.61}(SO_4)_{1.75}\cdot 1.01H_2O$
PG1	0.01	0.01	$CaEu_{0.0021}Na_{0.26}(SO_4)_{1.13}(PO_4)_{0.0021}\cdot 1.89H_2O$
PG2	0.5	0.5	$CaEu_{0.28}Na_{0.42}(SO_4)_{1.25}(PO_4)_{0.255}\cdot 2.14H_2O$

511

512

513 **Table 2.** Phase fractions of gypsum and bassanite in samples based on Rietveld refinements and
514 the distribution of water content obtained by TG measurements between the two.

Sample	$CaSO_4$ (mol)	Based on Rietveld analysis		Based on TGA and Rietveld analysis	
		Moles of gypsum	Moles of bassanite	Water of crystallization(mol)	Adsorbed water (mol)
GS 1	1	1	0	2	0.05
GS 2	1	0.12	0.88	0.68	0.33
PG 1	1	0.88	0.12	1.82	0.07
PG 2	1	0.65	0.35	1.475	0.665

515

516

517 **Table 3.** Thermochemical data used for the calculation of enthalpy of formation of Eu-doped
518 gypsum-phosphogypsum samples

Phase	Drop solution enthalpy* (kJ/mol)	Reference
CaO	-90.3±1.8	A. Navrotsky, J Am Ceram Soc (2014)
Eu_2O_3	-129.24±2.12	A. Navrotsky, J Am Ceram Soc (2014)
Na_2O	-217.56±4.25	A. Navrotsky, J Am Ceram Soc (2014)
P_2O_5	-164.6±0.85	A. Navrotsky, J Am Ceram Soc (2014)
SO_3	-203.7±4.09	A. Navrotsky, J Am Ceram Soc (2014)
$CaSO_4$	108.25±1.20	J. Majzlan, Geochimica et Cosmochimica Acta, 2002
Na_2SO_4	155.7±2.30	C. Drouet, Geochimica et Cosmochimica Acta, 2003
$Eu_2(SO_4)_3$	265.05±4.60	Present work
$EuPO_4$	139.87±1.43	S. Ushakov, J Mater Res, 2001
H_2O	68.98±0.1	calculated from heat capacity

519

520 * in molten $3Na_2O{\cdot}4MoO_3$

521

This is a preprint, the final version is subject to change, of the American Mineralogist (MSA)
Cite as Authors (Year) Title. American Mineralogist, in press.
(DOI will not work until issue is live.) DOI: http://dx.doi.org/10.2138/am-2016-5684

522 **Table 4**. Thermochemical data of Eu – gypsum and phosphogypsum samples

Sample	Drop solution enthalpy (kJ/mol)	ΔH_f from oxides (kJ/mol)	ΔH_f from mixture of sulfates (anhydrous) and phosphate (kJ/mol)	ΔH_f from mixture of gypsum/bassanite and phosphate (kJ/mol)
GS 1	299.60±1.88	-511.74	-27.78	1.46
GS 2	256.05±1.85	-719.18	9.00	23.15
PG 1	263.16±3.22	-482.39	-3.65	23.53
PG 2	266.43±2.19	-549.17	61.69	84.94

523

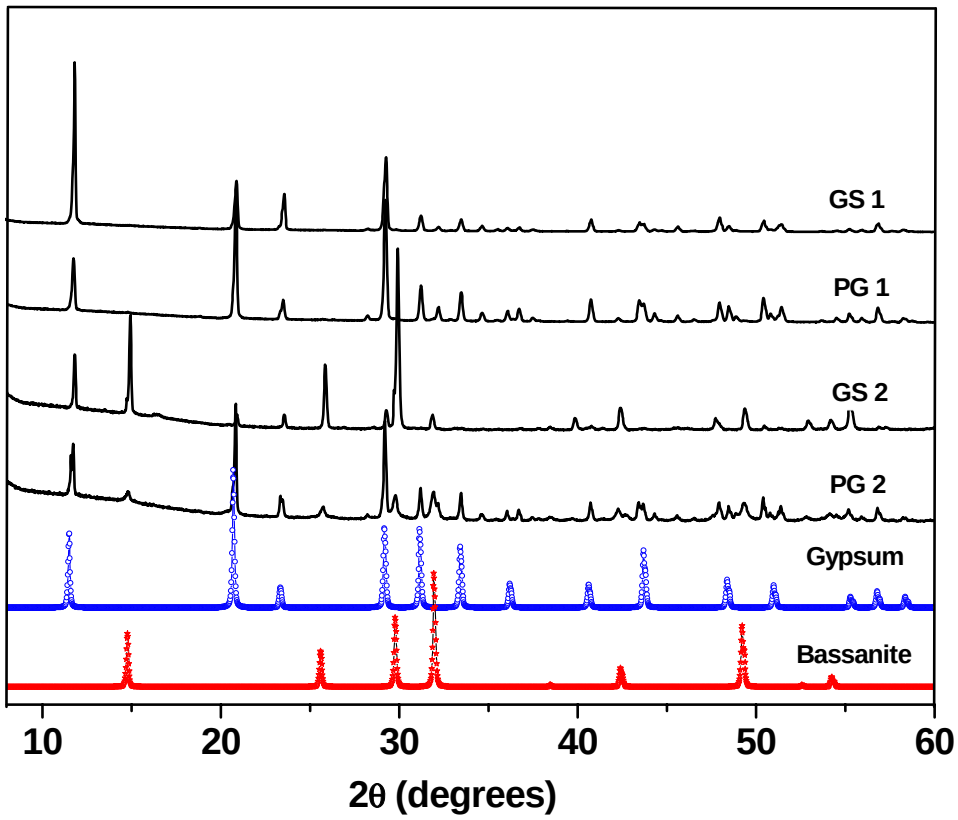

Figure 1. PXRD patterns of all the samples stacked with the simulated patterns of gypsum and bassanite

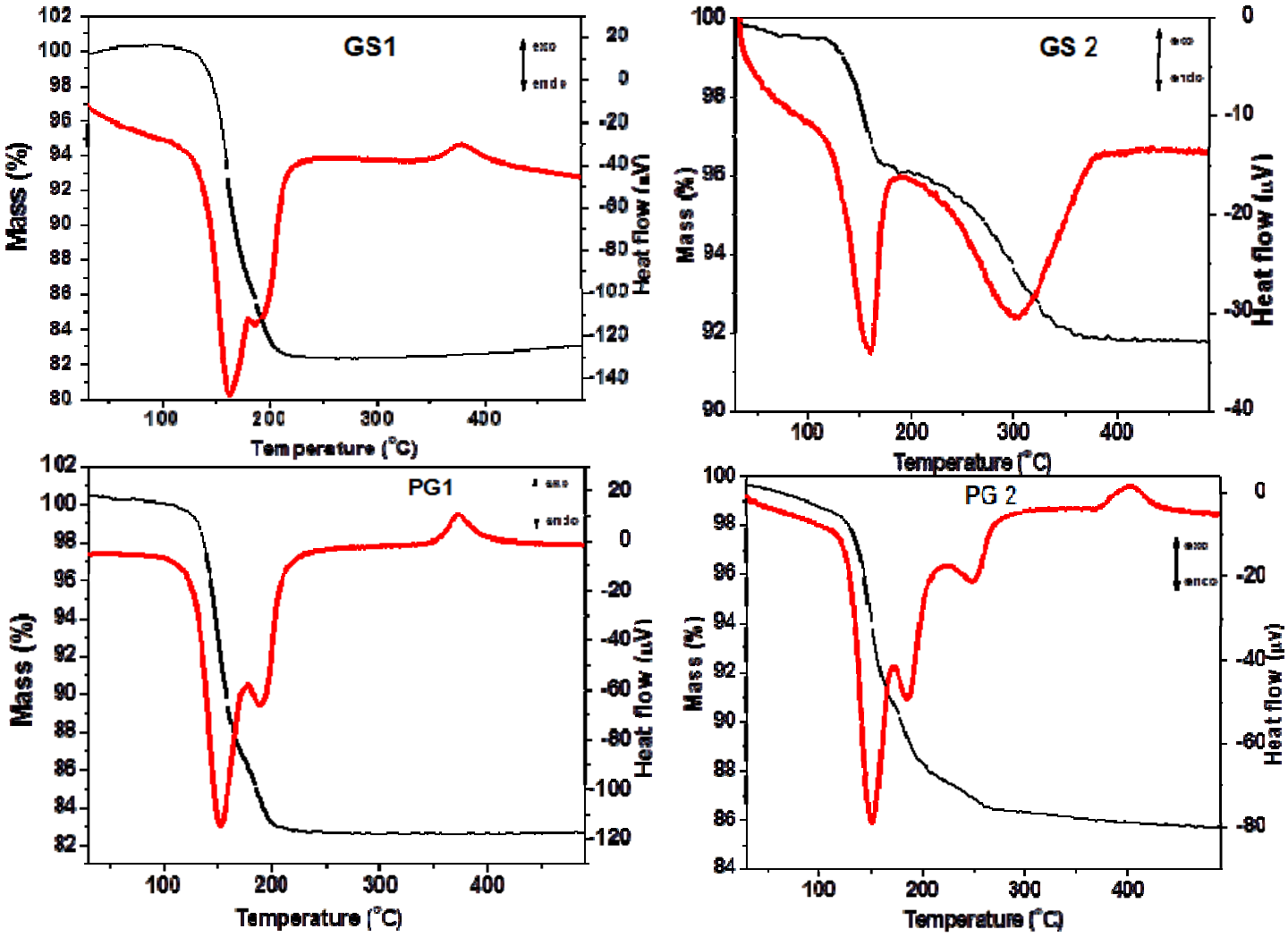

537 **Figure 2.**TG-DSC curves of Eu doped gypsum and phosphogypsum samples

538

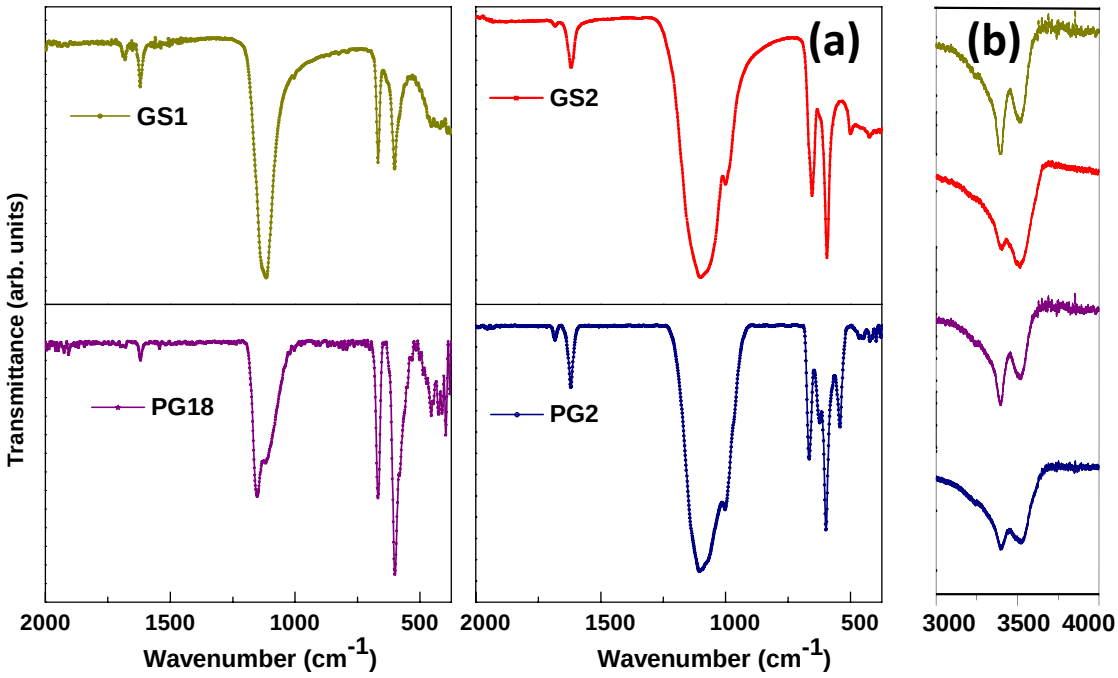

Figure 3. ATR spectra of all the four samples between (a) 400 – 2000 cm^{-1} showing vibrations corresponding to sulfate/phosphate and (b) 3000 – 4000 cm^{-1} showing vibrations due to H_2O.

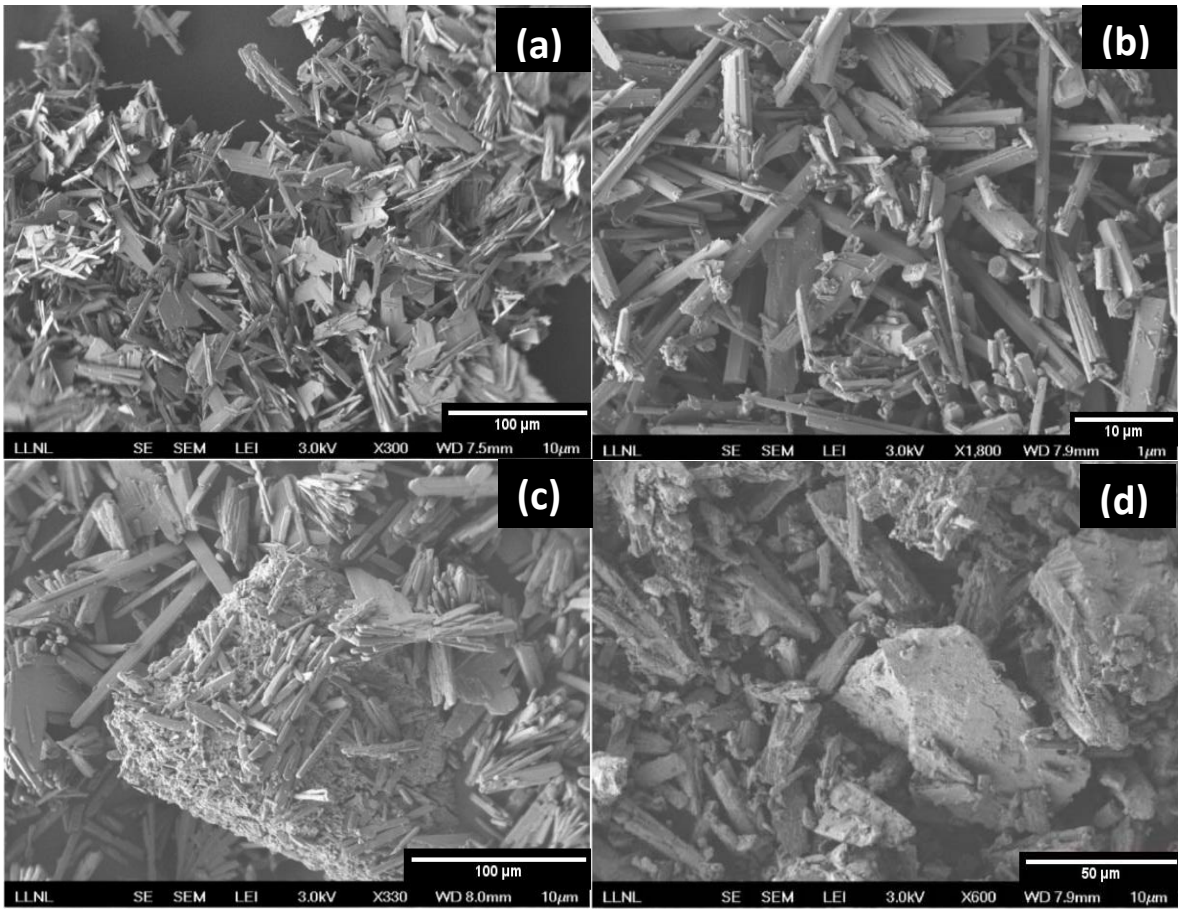

Figure 4. SEM images of (a) GS 1, (b) GS 2, (c) PG 1 and (d) PG 2

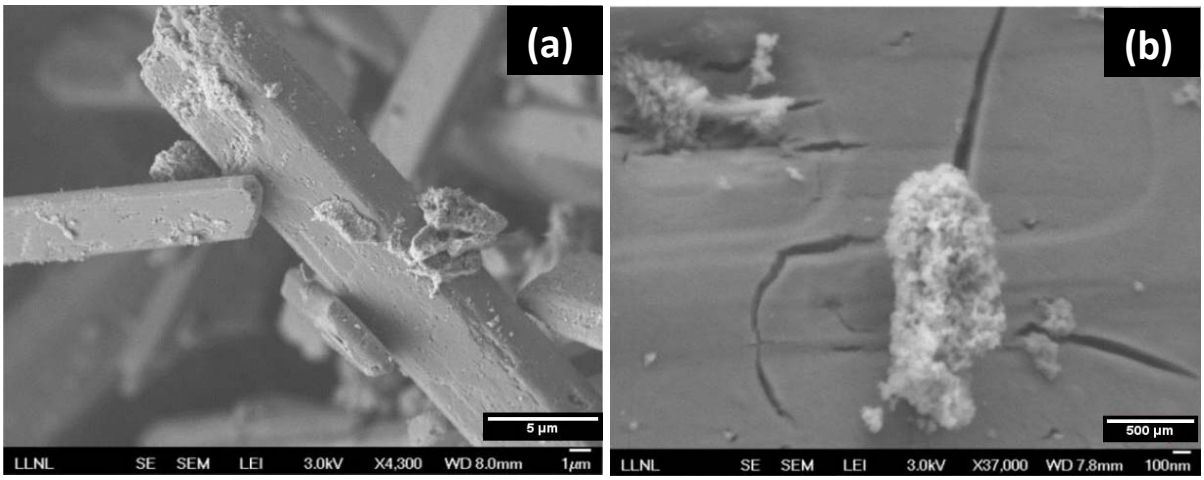

Figure 5. SEM image of (a) PG 2 sample showing surface adsorbed layer of Eu phase and (b) PG 1 sample showing Eu – rich particles with no faceted morphology

584

$CaEu_yNa_z(SO_4)_m \cdot nH_2O\ (s) \rightarrow CaSO_4\ (sol) + (y/2)Eu(SO_4)_3\ (sol) + (z/2)Na_2SO_4\ (sol) + nH_2O\ (sol)$	H1
$CaSO_4\ (s) \rightarrow CaSO_4\ (sol)$	H2
$Eu_2(SO_4)_3\ (s) \rightarrow Eu_2(SO_4)_3\ (sol)$	H3
$Na_2SO_4\ (s) \rightarrow Na_2SO_4\ (sol)$	H4
$H_2O\ (s) \rightarrow H_2O\ (l)$	H5
$xCaSO_4\ (s) + (y/2)Eu(SO_4)_3\ (s) + (z/2)Na_2SO_4\ (s) + nH_2O\ (s) \rightarrow CaEu_yNa_z(SO_4)_m \cdot nH_2O\ (s)$	H6
$\Delta H_f = H6 = -H1+H2+(y/2)H3+(z/2)H4+H5$	

593

594 **Figure 6.** Thermochemical cycle used for the calculation of enthalpy of formation values (ΔH_f)

595 of Eu-gypsum samples from a mixture of anhydrous sulfate and water

596